ACS APPLIED MATERIALS & INTERFACES

Research Article

www.acsami.org

Fabrication of Oxidation-Resistant Metal Wire Network-Based Transparent Electrodes by a Spray-Roll Coating Process

S. Kiruthika,[†] Ritu Gupta,[‡] Aman Anand,[†] Ankush Kumar,[†] and G. U. Kulkarni*[,§,⊥]

[†]Chemistry & Physics of Materials Unit and Thematic Unit of Excellence in Nanochemistry, Jawaharlal Nehru Centre for Advanced Scientific Research, Jakkur P.O., Bangalore 560064, India

[‡]Department of Chemistry, Indian Institute of Technology Jodhpur, Jodhpur 342011, Rajasthan, India

[§]Centre for Nano and Soft Matter Sciences, Jalahalli, Bangalore 560013, India

Supporting Information

ABSTRACT: Roll and spray coating methods have been employed for the fabrication of highly oxidation resistant transparent and conducting electrodes (TCEs) by a simple solution process using crackle lithography technique. We have spray-coated a crackle paint-based precursor to produce highly interconnected crackle network on PET roll mounted on a roll coater with web speed of 0.6 m/min. Ag TCE with a transmittance of 78% and sheet resistance of ∼20 Ω/□ was derived by spraying Ag precursor ink over the crackle template followed by lift-off and annealing under ambient conditions. The Ag wire mesh was stable toward bending and sonication tests but prone to oxidation in air. When electrolessly coated with Pd, its robustness toward harsh oxidation conditions was enhanced. A low-cost transparent electrode has also been realized by using only small amounts of Ag as seed layer and growing Cu wire mesh by electroless method. Thus, made Ag/Cu meshes are found to be highly stable for more than a year even under ambient atmosphere.

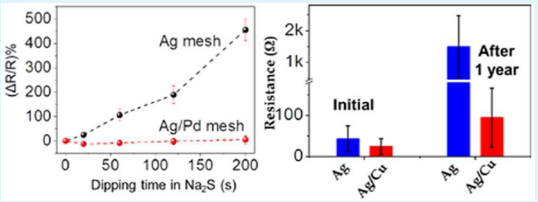

KEYWORDS: *Transparent conducting electrodes, crackle template, Ag wire network, roll coating, spray coating, oxidation resistant*

1. INTRODUCTION

Transparent conducting electrodes (TCE) with excellent optoelectronic properties are key components in various devices such as touch screens,[1,2] organic solar cells,[3] smart phones,[4] etc. Large area TCEs are increasingly in demand because of the increasing size of the active parts of these devices,[5] and in this context, large area manufacturing techniques such as roll-to-roll gain significance. For example, large area flexible organic tandem solar cell modules have been achieved through a roll-to-roll process, recently.[6,7] Perovskite solar cells fabricated by slot-die coating technique yielded ∼12% conversion efficiency, showing the possibility toward mass production using roll-to-roll method.[8] The roll-to-roll system has been used to deposit/grow materials such as carbon nanotubes (CNT) on aluminum strips which find use as electrodes in battery and supercapacitors.[9,10] In most optoelectronic devices, the use of a transparent electrode is a must. It has become fashionable to make even the non-optoelectronic devices, transparent.[11−13] Obviously, it requires high-volume, large-area manufacturing of transparent conducting electrodes. In this direction, there have been efforts to make roll-to-roll TCEs with indium tin oxide (ITO), the most commonly used transparent material.[14,15] Limitations of ITO such as brittleness, high material and process cost, and chemical instability have prompted the search for alternate materials amenable for large area manufacturing.

With the recent successes in new generation materials such as graphene,[16,17] conductive polymers,[18] metallic grids,[19] random networks of carbon nanotubes (CNTs),[20] metal nanowire networks (Ag, Cu),[21,22] their hybrids,[23−26] etc., scalability and cost effectiveness of the TCE are set to be the next achievable goals. In comparison to ITO, new generation materials and their hybrids are highly versatile for large scale fabrication. Undoubtedly, Ag and Cu nanowire electrodes can be easily produced by additive coating method over large areas by roll coating. The hybrid nanostructures are also produced by multiple coating steps to address the issues of high surface roughness, poor adhesion to substrate, high junction resistance between the nanowires, and nonuniform distribution of nanowires on substrate. Despite the fact that fabrication of hybrid electrodes involves extensive processing and multiple optimization steps, it is still considered to be highly promising. For example, Ag nanowires embedded in graphene or in PEDOT:PSS are being obtained by a roll-to-roll process.[24,25]

Templating methods such as bubble template,[27] electrospun fibers,[28] etc., are considered superior compared to networks obtained by simple coating of the presynthesized nanowires on a substrate. The templating methods offer well-defined fill-factors across the substrate area as well as seamless junctions. Among the templating methods, metal meshes have been produced using a rather simple process involving crack templates.[29−36] However, considering the advantages of metal

Received: September 1, 2015
Accepted: November 18, 2015
Published: November 18, 2015

DOI: 10.1021/acsami.5b08171
ACS Appl. Mater. Interfaces 2015, 7, 27215−27222

mesh electrodes over nanowires and hybrid electrodes, it is worthwhile to explore the possibility for scale-up of template-based methods. There are no reports for the scalability of template-based methods, since it is a highly challenging to obtain uniform templates over large areas. We have previously demonstrated crack lithography method in which metal meshes can be derived over areas limited only by the size of metal evaporation chamber.[32,33,35] The process can be extended to roll-to-roll only if metal can be brought by complete solution based processing. This work aims at scalability of crack lithography method by exploring different strategies shown in Scheme 1 that includes solution based deposition of metal in crackle grooves by a spray and roll coating process.

Scheme 1. Schematic Representation of Different Methods Adopted for Solution-Based Processing of Metal Electrodes from Crackle Lithography[a]

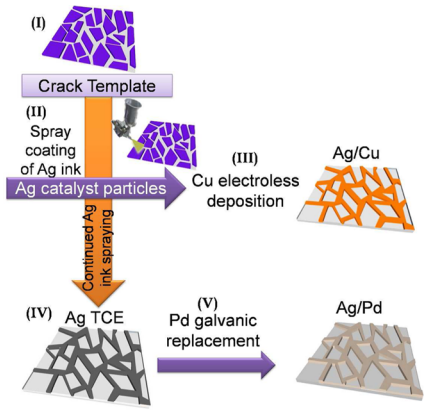

[a]Interconnected crack template (I) was obtained by spray coating crackle precursor over PET substrate. In step (II), Ag precursor ink was spray coated over template under ambient conditions. With a minimal usage of Ag as a seed layer in crackle grooves, the desired connectivity and conductivity was brought in by depositing Cu through an electroless process (III). Alternatively by continuing Ag deposition, highly interconnected conducting Ag wire network was obtained (IV). Highly oxidation resistant Ag/Pd mesh was obtained by a simple galvanic replacement process (V).

2. EXPERIMENTAL SECTION

Fabrication of Crackle Template by Roll Coating. Commercially available silica nanoparticle-based dispersion (Premium Coatings and Chemicals, India) was used to obtain crackle template on PET substrate. The nanoparticle based dispersion was diluted with diluter to achieve the required concentration of 0.6 g/mL. The dispersion was always kept in an airtight bottle in order to avoid evaporation of organic solvents. The crackle precursor (CP) was spray coated at the nitrogen pressure of ∼25 psi on a clean and dried PET substrate. The custom designed roll coater as shown in Figure 1 was set to rotate at 2 rpm. The crackle precursor was spray deposited manually at a fixed distance of 5 cm with a 135A airbrush with 0.2 mm nozzle from United Traders, Bangalore. The crackle widths were tuned by increasing the wet layer thickness, controlled by number of passes of spray coating. The substrate was then left to dry in air while a crackle network pattern formed spontaneously in the coated layer. The crackle precursor formulations contain film forming agents that enable smooth and uniform coating of the template over large areas.

Fabrication of Ag Mesh. Ag precursor ink purchased from Kunshan Hisense Electronics Co., Ltd., China, 3 times diluted with isopropanol (IPA), was sprayed on the crackle network on PET maintained at 110 °C on the roller drum. All roll and spray coatings

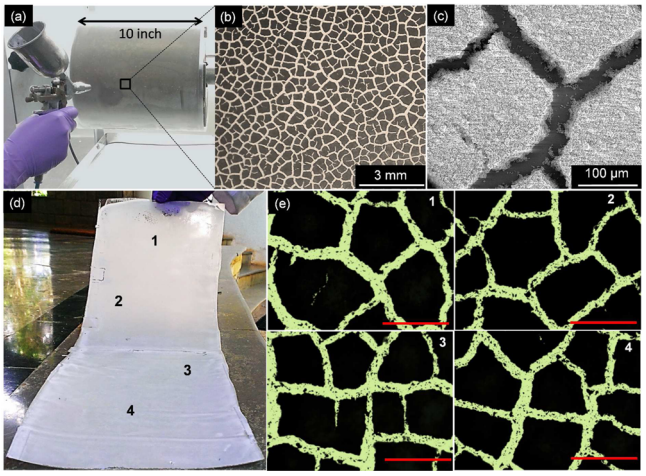

Figure 1. (a) Photograph demonstrating the formation of crackle template over large area PET substrate using the spray coat on roll technique. (b) Optical micrograph and (c) SEM image of thus formed interconnected crackle network. (d) Photograph of a roll of crackle template. The scratches observed are mainly due to template handling during photography. Few places on the sides are marks of the scotch tape used for sticking the PET substrate onto the roller drum. (e) Optical microscopic images of crackle template captured from different positions of the sample. Scale bar is 300 μm.

were performed in separate enclosure connected with exhaust in order to protect from strong smell of Ag precursor ink decomposition. According to the area of crackle template, appropriate volume of Ag ink was taken and was sprayed using spray gun. The spray gun was kept 5 cm away from the template for uniform spraying. The PET sheet carrying crackle template was detached from the roll coater and the template was removed by simple mechanical peeling. After the removal of template, Ag precursor ink was completely converted to metallic Ag by annealing at 140 °C for about 10 min in order to remove organic moieties from the Ag precursor ink.

Fabrication of Ag/Pd Mesh. Pd acetate (5.5 mM) in acetic acid was diluted with 20 mL of distilled water and maintained at 60 °C while depositing Pd by galvanic displacement over the Ag mesh. The deposition was carried out for 25 min.

Fabrication of Ag/Cu Mesh. To fabricate Ag/Cu TCE on PET substrate, Ag seed layer was formed on crackle grooves by spraying 5 times diluted Ag ink. After the removal of template and complete conversion to metallic Ag, it was dipped in Cu plating solution. The Cu plating bath was composed of solution A (1.5 g of $CuSO_4$ and 7 g of sodium potassium tartrate mixed with 2 g of NaOH in 50 mL of distilled water) and formaldehyde as solution B. A freshly prepared plating solution (A:B = 10:1) was used for Cu electroless deposition on Ag seed layer. The plating process was stopped by taking out the sample from bath and rinsing with distilled water.

Characterization. Scanning electron microscopic (SEM) images were obtained using a Nova NanoSEM 600 instrument (FEI Co., The Netherlands). Energy-dispersive spectroscopy (EDS) analysis was performed with an EDAX Genesis instrument (Mahwah, NJ) attached to the SEM column. The EDS mapping was performed at 10 kV. The optical microscopic images were obtained using the microscope from Laben, India. Wyko NT9100 Optical Profiling System (Bruker, USA) was used for measuring height and roughness of formed films. X-ray diffraction (XRD) measurements were performed on a Miniflex (Rigaku, Japan). Transmittance spectra were measured using a Perkin−Elmer Model Lambda 900 UV/visible/near-IR spectrophotometer from 400−1200 nm. Thermo gravimetric analysis (TGA) was carried out using a Mettler Toledo, TG-850 set up, with sample weight of 33.7 mg in ambient atmosphere in the temperature range of 24−200 °C at a heating rate of 2 °C/min. The resistance of TCE was measured using a 4-Point Probe Station (Techno Science Instruments, India). Mechanical tests were performed by connecting electrical leads

DOI: 10.1021/acsami.5b08171
ACS Appl. Mater. Interfaces 2015, 7, 27215−27222

to DMM viewer software to record the change in resistance by interfacing a multimeter (Test Link, India) with a computer while performing test. A sonicator from Elmasonic P was used to perform ultrasonication test with a maximum power and at a frequency of 30 kHz. The bending tests were performed using a custom designed setup. After making contact pads with silver epoxy, one side of electrode was fixed, whereas other was kept movable to attain different bending radii with a help of screw gauge.

3. RESULTS AND DISCUSSION

To develop a reliable method for producing solution-processed low-cost TCE over large area, we have employed a custom designed roll coater. The silica nanoparticle based dispersion (CP) used for crack template formation was sprayed directly at the pressure of 25 psi on PET substrate wrapped around a 10 in. roller rotating at 2 rpm under ambient conditions (Figure 1a). The spray continued for over 5 passes such that the desired thickness of ~35 μm (see Figure S1) for the interconnected crackle template could be achieved. The processing speed was 0.6 m/min. Once the precursor dried completely, highly interconnected spontaneously formed cracks were observed as shown in Figure 1b and c. The crackle widths were typically in the range of 50−150 μm. The thickness of the dried CP layer is dependent on the number of spray passes while other experimental conditions remain similar. An increase in the number of passes (3−15) led to higher thickness of the dried CP and hence wider cracks (150−180 μm) (see Figure S2). These cracks were down to the substrate which we term as crackles, and these crackle patterns were used as templates for metal deposition. Photograph of thus formed crackle template on a roll of PET is shown in Figure 1d. The optical micrographs of crackles formed at different positions are shown in Figure 1e.

The Ag mesh was fabricated on transparent and flexible PET substrate following the procedures as shown in schematic in Figure 2. Briefly, Ag ink (3 times diluted with IPA) was sprayed (25 μL/cm^2) on the crackle network on PET maintained at 110 °C on the roller drum. After 10 min of coating, the PET sheet carrying the crackle template was detached from the roller and the template was removed by simple mechanical peeling using adhesion tape. The dried ink pattern on PET was converted to metallic Ag by annealing at 140 °C for about 10 min (Figure S3). This is confirmed by XRD measurement in Figure 2a, showing that the peaks match well with those of metallic Ag (JCPDS PDF, 89−3722). From the SEM image in Figure 2b, we see that the formed Ag mesh is interconnected with seamless junctions in a single plane. The width of Ag mesh is typically 50−150 μm. The optical transmittance spectra of Ag meshes of different widths are shown in Figure 2c. Transmittance spectra of meshes are constant in visible and near IR regions useful for display and solar applications, respectively. The transmittance of Ag mesh at 550 nm varies from 78 to 53% and sheet resistance from 21 to 5 Ω/□. Figure 2d shows the optical micrographs of Ag meshes with different widths on PET substrate. Interconnectivity between the meshes increases with increase in wire widths and thus leads to lower sheet resistance.

The haze value is defined as $H = \Delta T/T_{dif} \times 100$, where $\Delta T = T_{dif} - T_{sp}$; T_{dif} is diffusive transmittance and T_{sp} is specular transmittance. The haze values of Ag meshes of different widths estimated from specular and diffusive transmittance measurements are found to be in the range 5−11% (see Figure 3a, b). The sheet resistance and transmittance values randomly measured from across 100 cm^2 area of Ag mesh are shown in Figure 3c. The uniformity in the measured parameters is thus

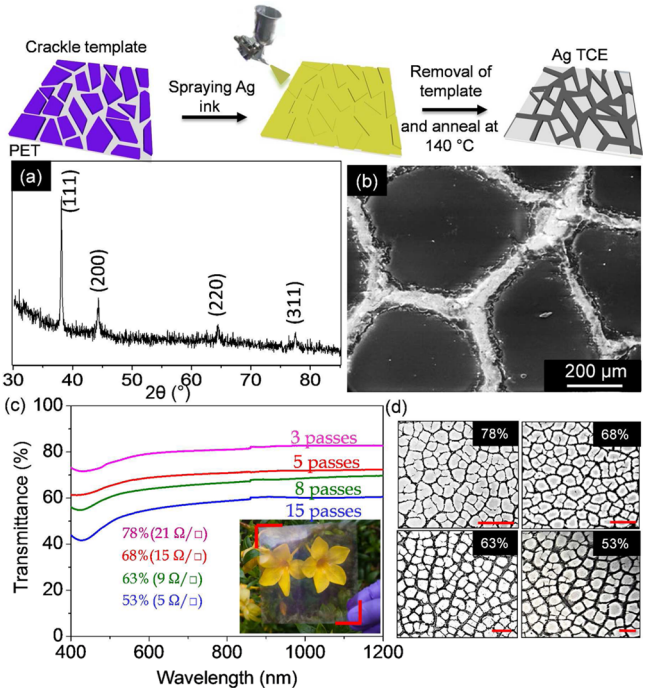

Figure 2. Schematic illustration of the key steps involved in the fabrication of Ag-TCE. (a) X-ray diffraction pattern of Ag mesh prepared by spraying Ag molecular ink. (b) SEM image of Ag mesh. (c) Specular optical transmittance of Ag mesh prepared from crackles of different widths. The sheet resistances of the samples are mentioned in parentheses. Photograph of the prepared TCE with 78% transmittance at 550 nm is shown as an inset. (d) Optical micrographs of Ag mesh of different widths. Scale bar is 1 mm.

evident. It may be noted that spray coating being directional avoids unnecessary spreading of the ink. Our initial attempts by drop coating the Ag ink resulted in diffusion of the ink beneath the crackle template. This greatly affected the transmittance of the TCE because of uncontrolled mesh widths. The histogram comparing the width of crackles and Ag meshes fabricated thereof by spray coating is shown in Figure S4. Further annealing at a moderate temperature of 110 °C while spraying enables quick evaporation of the solvents, thereby avoiding spreading of the ink beneath the crackle groove and also does not hinder in the subsequent lift-off process (see Figure S5).

Metallized Ag on PET with the experimental conditions used is known to adhere well on the substrate.[6,37] The mechanical stability of the metallized Ag in crackle network was examined (Figure 4) using the standard scotch tape adhesion test and by repeated bending while monitoring the resistance. As shown in Figure 4a, the Ag mesh-based TCE showed minimal changes in the resistance (<0.5%) after performing the adhesion test. In addition, we have performed sonication test by immersing Ag mesh in an ultrasonic water bath. The variation in resistance was less than 1% as shown in Figure 4b. These tests clearly suggest that the Ag mesh has good adhesion with the PET substrate. In order to examine the stability of Ag mesh in the context of flexible electronics, the Ag/PET was subjected to different bending radii. In spite of being bent to 1.5 mm, the variation in resistance was only ~1% (Figure 4c). Although, the mesh was subjected to 500 bending cycles with 1.5 mm radius, the change in the resistance remained within 5%, which demonstrates its robustness (Figure 4d). Importantly, the above tests required no encapsulation of the TCE.

DOI: 10.1021/acsami.5b08171
ACS Appl. Mater. Interfaces 2015, 7, 27215−27222

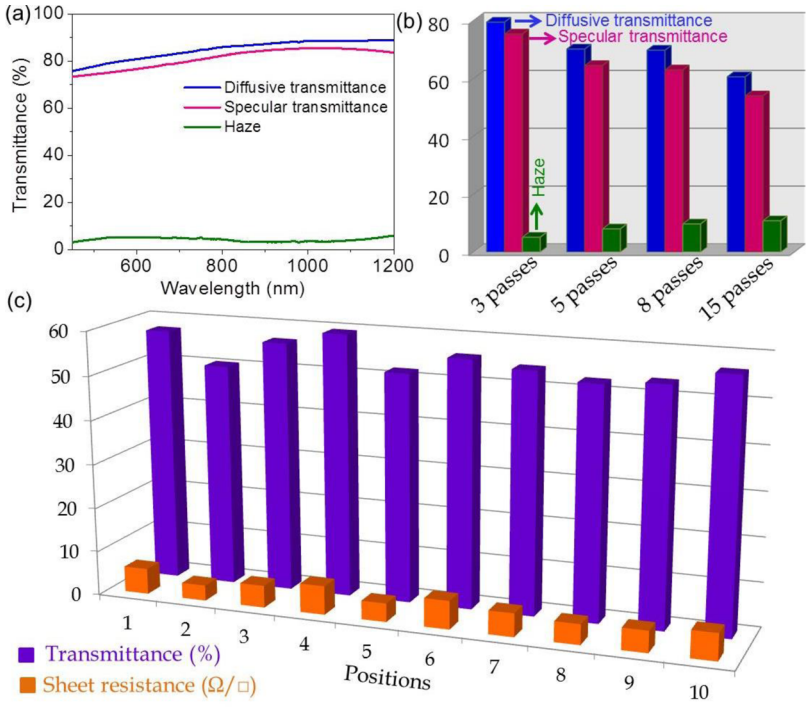

Figure 3. (a) Diffusive and specular transmittance along with calculated haze values of the Ag mesh fabricated from a crackle template (3 spray passes). (b) Histogram showing transmittance and haze value of various Ag mesh widths. (c) Sheet resistance and transmittance measured across 100 cm^2 area of Ag TCE prepared from a template (15 passes). Each measurement was done over 10 × 5 mm^2 randomly chosen areas.

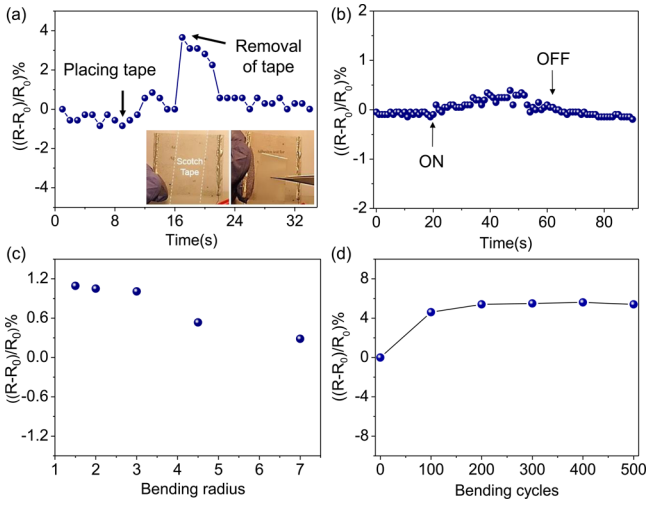

Figure 4. Relative variations in the resistance of the Ag mesh during (a) the scotch tape adhesion test, (b) sonication test, (c) bending to different radii, and (d) 500 bending cycles to radius of 1.5 mm. The photographs in the inset in a show the scotch tape pasted over the Ag mesh and while peeling off.

In general, Ag and Cu nanowires tend to get oxidized in atmospheric conditions due to chemical instability which leads to deterioration of conductivity and thus the performance of optoelectronic devices.[38,39] Tarnishing of Ag is very harmful for electronic circuits in certain environments. Even in the presence of ppm level sulfide content in the atmosphere, silver sulfide nanoparticles get formed as a shell over Ag nanowires increasing the surface roughness.[38,40] With time, sulfide shell thickness increases at the cost of Ag core leading to higher resistance of the nanowire network.[41] Therefore, it is essential to suppress the oxidation of nanowires in order to enhance the long-term stability. Recent studies have shown that protective layer of reduced graphene oxide (r-GO) or graphene over Ag or Cu nanowires coated by dip-coating,[42] spray-coating,[43] spin-coating,[44] or dry transfer processes[45] prevent its oxidation by forming passivation layer. These additional passivation coatings not only increase number of process steps and also the cost of TCEs. Among the many protecting layers, thin coating of a noble or seminoble metal by solution processing is highly promising as the coated metal can bring in highly resistant property to the nanowire. The surface stability of semi noble metal like Ag is improved by encapsulating with noble metals by simple galvanic replacement method.[46,47] Cui and co-workers have demonstrated that junction resistance between Ag nanowires could be reduced by encapsulating Au by galvanic replacement.[48] Besides being highly stable, the neutral gray color of Pd is highly desirable for display applications. Hence we adopted a simple process of coating Pd from a liquid carrier that produced a Pd-coated Ag mesh making it highly resistant to oxidation processes. The schematic in Figure 5 illustrates the fabrication process. SEM image of Ag/Pd mesh after galvanic displacement is shown in Figure 5a. EDS mapping of mesh (Figure 5b, c) clearly shows the presence of protective layer of Pd shell. The transmittance of Ag/Pd mesh is lower than Ag mesh to some extent (Figure 5d), as nonspecific deposition is unavoidable in case of solution process. The coating of Pd over the Ag mesh slightly increases the resistance of mesh (14 Ω/□ to 16 Ω/□) likely due to the higher resistivity of Pd. Oxidation resistance of Ag/Pd was demonstrated by dipping the mesh in Na_2S solution. The Na_2S treatment has been performed as an accelerated test for estimating the stability of the TCE, and in this context, the performances of Ag/Pd with Ag have been compared. Schematic of the process is shown as the inset in Figure 5e. Despite the extreme oxidation environment, the resistance of the Ag/Pd mesh toward aqueous Na_2S solution

DOI: 10.1021/acsami.5b08171
ACS Appl. Mater. Interfaces 2015, 7, 27215−27222

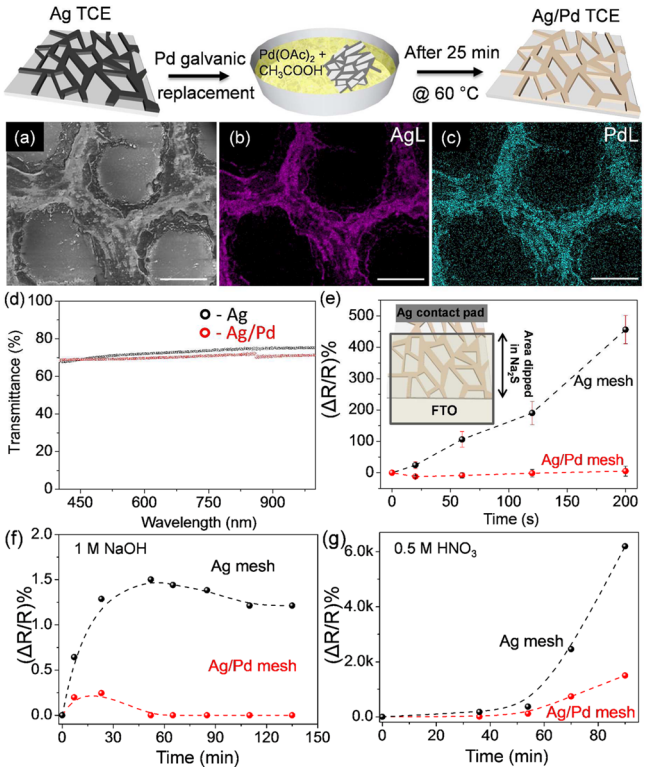

Figure 5. Schematic illustrating the fabrication of Ag/Pd mesh. (a) SEM image of Ag/Pd mesh. EDS mapping of mesh showing the presence of (b) Ag and (c) Pd. Scale bar is 100 μm. (d) Transmittance spectrum of Ag and Ag−Pd meshes. (e) Variation in electric resistance of Ag and Ag/Pd meshes vs dipping time in 50 mM Na_2S solution. Inset is the schematic of the process. To avoid exposure of Ag contacts to the sulfidic solution, only one Ag contact was taken from the network such that rest of it was free to be dipped in the solution. After dipping in solution for designated time followed by drying, the dipped part of the network was brought in contact with a fluorine-doped tin oxide (FTO) plate, which served as second contact. (f, g) Relative variation in resistance of the Ag and Ag/Pd meshes when exposed to 1 M NaOH and 0.5 M HNO_3, respectively.

was excellent and was superior to that of the Ag mesh (Figure 5e). After 200 s exposure, the resistance of the Ag mesh drastically increased to 450% whereas that of Ag/Pd mesh varied within 5%. Even after dipping for 1000 s, the resistance of the Ag/Pd mesh was less than a kΩ, whereas the resistance of the Ag mesh reached several GΩs. From the SEM images, we observe that there is no major change in morphology of Ag and Ag/Pd meshes before and after dipping in the Na_2S solution. It is noteworthy that the XRD pattern of the Ag mesh showed distinct peaks of Ag_2S (see Figures S6 and S7). Further, the stability of the Ag and Ag/Pd meshes have been tested under HNO_3 and NaOH solutions (Figure 5f, g). The Ag/Pd mesh showed relatively long-term chemical stability superior to Ag mesh in both conditions. The simple process adopted here to enhance the stability can be used as a general strategy to improve the throughput and performance of transparent electrodes.

Although Ag offers versatile inks to work with, other cheaper metals such as Cu can only be brought into the TCE fabrication in a subsequent step using seed layer. In recent literature,[49−53] wearable conducting electrodes for various applications have been reported fabricated through simple seed layer formation followed by electroless deposition process. In our attempts to reduce Ag usage, we followed a simple electroless method wherein only a small quantity of dilute Ag ink (dilution, 5 times and volume, 15 μL/cm^2) was initially sprayed and annealed which produced enough concentration of Ag catalyst nanoparticles (Figure S8) for Cu deposition. SEM image of Ag seed layer is shown in Figure 6a. An inexpensive metal like Cu (100

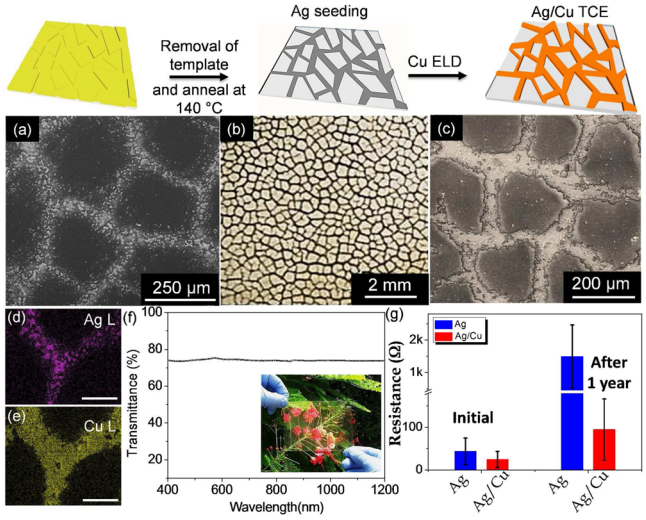

Figure 6. Schematic representation of the fabrication of Ag seeded Cu TCE. (a) SEM image of Ag seed layer. (b) Optical micrograph and (c) SEM image of Ag/Cu TCE. (d, e) Energy-dispersive X-ray spectroscopy images of Ag/Cu mesh on PET. Scale bar is 100 μm. (f) Transmittance spectrum of Ag/Cu mesh on a flexible PET substrate. Inset is the photograph of flexible transparent Ag/Cu electrode. (g) Resistance of Ag- and Ag/Cu-based TCEs after one year of storage in ambient atmosphere.

times lower cost than Ag) was electroless deposited over Ag seed layer. The Cu metal was selectively deposited over Ag by dipping the PET substrate containing Ag network in a plating bath for 5 min without any external voltage. Optical micrograph and SEM image of thus fabricated Ag/Cu mesh clearly shows a highly interconnected network with seamless junctions (Figure 6b, c). The uniform coating of Cu over Ag was further confirmed by EDS mapping as shown in Figure 6d, e. The root-mean-square (R_{rms}) roughness of the Ag/Cu mesh was found to be 43 nm (see Figure S9). A view of substrate carrying Ag/Cu mesh proves its transparency to the visible light (Figure 6f). The transmittance at 550 nm was 76% for a low sheet resistance of 9 Ω/□. Large area uniformity of the prepared Ag/Cu mesh is illustrated in Figure S10. To explore the effect of Cu deposition time on the sheet resistance, we carried out the deposition process with increasing time duration, from 5 to 15 min. As shown in Figure S11, the sheet resistance values gradually decreased from 9 Ω/□ to 1.5 Ω/□ but beyond 5 min of deposition, nonspecific deposition of Cu occurred which greatly affected the transmittance as well as adhesion of Cu to the substrate. Besides reducing the cost of TCE fabrication, the Cu shell on Ag also enhances the stability of mesh. This is clearly seen from the sheet resistance values measured from the prepared meshes initially and after a year of storage in ambient atmosphere. Though the Ag/Cu TCE was exposed to ambient atmosphere for one year, it had excellent stability as shown in Figure 6g. In contrast, Ag TCE degraded significantly because of ease of oxidation and highly porous surface unlike Ag/Cu (see Figure S12). Ag/Cu mesh being more stable is bit

DOI: 10.1021/acsami.5b08171
ACS Appl. Mater. Interfaces 2015, 7, 27215−27222

surprising. However, the porosity of the wire mesh also plays an important role. As shown in Figure S12, the Ag/Cu mesh is less porous compared to Ag mesh. In the presence of large number of pores and increased surface area, Ag tends to get oxidized relatively rapidly. The pores formed in Ag are filled up by Cu in a latter step, thus bringing additional stability against oxidation.

In our previous studies related to crackle lithography, the TCEs were realized by depositing metal on crackle grooves by physical deposition process except an attempt where Cu TCE was fabricated using Au and Pd as seed layer.[33] Au seeding was done using sputtering process which demands vacuum system. In general, thin layer of noble metals is coated for high stability rather than as a seed layer. In this work, we have used Pd as protection layer for Ag against oxidation environment. Also we have employed Ag as seed layer from spray coating of the precursor to successfully grow Cu wire meshes. Thus, the present work is the first step toward large scale production of TCEs using roll coating processes. The novelty of this work is that it is a complete solution-based recipe that is cost-effective and adaptable for roll-to-roll processing. Unlike spin coating or rod coating, spray roll process is significant for industrial processing.

CONCLUSIONS

In summary, we have attempted to upscale the fabrication of cost-effective TCE by adopting roll and spray coating techniques in a crackle template method. The processing speed for the template fabrication was 0.6 m/min under ambient conditions. However, the web speed could be improved with further optimization of processing parameters such as by increasing spray volume and faster drying conditions. These completely solution processed Ag, Ag/Pd, and Ag/Cu mesh-based TCEs have shown superior chemical and mechanical robustness. This method generates metal meshes adhering well to the PET substrate with seamless metal junctions and high degree of interconnectivity. The Ag/Cu meshes produced in this study exhibited low sheet resistance (9 Ω/□) with high transmittance (~80%) which could be employed in a wide range of flexible and low-cost devices. In addition, Pd encapsulated Ag meshes have shown excellent stability toward oxidation. The developed process can be adopted as a general strategy to improve the throughput and performance of transparent electrodes, in place of relatively involved methods of nanowire encapsulation. The method adopted here opens up wide range of possibilities in future studies in terms of the metal or the material being deposited, which can be exploited for fine-tuning properties such as work function. The latter gains much significance in the context of optoelectronic device fabrication.

ASSOCIATED CONTENT

Supporting Information

The Supporting Information is available free of charge on the ACS Publications website at DOI: 10.1021/acsami.5b08171.

Optical profilometry of crackle template, crackle width versus thickness of crackle precursor, TGA of Ag precursor ink, variation in widths of crackle grooves and fabricated Ag meshes, photograph of Ag mesh TCE prepared at 130 °C, SEM images and XRD patterns of Ag and Ag/Pd meshes before and after Na_2S treatment for 1000 s, SEM images of Ag seed layer, optical profiler image of Ag/Cu mesh, change in sheet resistance and transmittance of Ag/Cu mesh over large area, dependence of sheet resistance on Cu deposition time, SEM images of Ag meshes and Ag/Cu meshes (PDF)

AUTHOR INFORMATION

Corresponding Author

*E-mail: kulkarni@jncasr.ac.in.

Notes

The authors declare no competing financial interest.

[⊥]On lien from Jawaharlal Nehru Centre for Advanced Scientific Research, Bangalore-560064, India.

ACKNOWLEDGMENTS

The authors thank Prof. C. N. R. Rao for his encouragement. The financial support from DST, India is gratefully acknowledged. S. K acknowledges DST-INSPIRE for fellowship. The authors acknowledge Mr. Karthikeya Srivastava for his initial assistance for assembling the roll coater.

REFERENCES

(1) Wu, H.; Kong, D.; Ruan, Z.; Hsu, P.-C.; Wang, S.; Yu, Z.; Carney, T. J.; Hu, L.; Fan, S.; Cui, Y. A Transparent Electrode Based on a Metal Nanotrough Network. *Nat. Nanotechnol.* **2013**, *8*, 421−425.

(2) Bae, S.; Kim, H.; Lee, Y.; Xu, X.; Park, J.-S.; Zheng, Y.; Balakrishnan, J.; Lei, T.; Ri Kim, H.; Song, Y. I.; Kim, Y.-J.; Kim, K. S.; Ozyilmaz, B.; Ahn, J.-H.; Hong, B. H.; Iijima, S. Roll-to-Roll Production of 30-Inch Graphene Films for Transparent Electrodes. *Nat. Nanotechnol.* **2010**, *5*, 574−578.

(3) Huo, L.; Liu, T.; Sun, X.; Cai, Y.; Heeger, A. J.; Sun, Y. Single-Junction Organic Solar Cells Based on a Novel Wide-Bandgap Polymer with Efficiency of 9.7%. *Adv. Mater.* **2015**, *27*, 2938−2944.

(4) Ryu, J.; Kim, Y.; Won, D.; Kim, N.; Park, J. S.; Lee, E.-K.; Cho, D.; Cho, S.-P.; Kim, S. J.; Ryu, G. H.; Shin, H.-A. S.; Lee, Z.; Hong, B. H.; Cho, S. Fast Synthesis of High-Performance Graphene Films by Hydrogen-Free Rapid Thermal Chemical Vapor Deposition. *ACS Nano* **2014**, *8*, 950−956.

(5) Kulkarni, G. U.; Kiruthika, S.; Gupta, R.; Rao, K. D. M. Towards Low Cost Materials and Methods for Transparent Electrodes. *Curr. Opin. Chem. Eng.* **2015**, *8*, 60−68.

(6) Gupta, R.; Walia, S.; Hösel, M.; Jensen, J.; Angmo, D.; Krebs, F. C.; Kulkarni, G. U. Solution Processed Large Area Fabrication of Ag Patterns as Electrodes for Flexible Heaters, Electrochromics and Organic Solar Cells. *J. Mater. Chem. A* **2014**, *2*, 10930−10937.

(7) Larsen-Olsen, T. T.; Andersen, T. R.; Andreasen, B.; Böttiger, A. P. L.; Bundgaard, E.; Norrman, K.; Andreasen, J. W.; Jørgensen, M.; Krebs, F. C. Roll-to-Roll Processed Polymer Tandem Solar Cells Partially Processed from Water. *Sol. Energy Mater. Sol. Cells* **2012**, *97*, 43−49.

(8) Hwang, K.; Jung, Y.-S.; Heo, Y.-J.; Scholes, F. H.; Watkins, S. E.; Subbiah, J.; Jones, D. J.; Kim, D.-Y.; Vak, D. Toward Large Scale Roll-to-Roll Production of Fully Printed Perovskite Solar Cells. *Adv. Mater.* **2015**, *27*, 1241−1247.

(9) Arcila-Velez, M. R.; Zhu, J.; Childress, A.; Karakaya, M.; Podila, R.; Rao, A. M.; Roberts, M. E. Roll-to-Roll Synthesis Of Vertically Aligned Carbon Nanotube Electrodes for Electrical Double Layer Capacitors. *Nano Energy* **2014**, *8*, 9−16.

(10) Oakes, L.; Hanken, T.; Carter, R.; Yates, W.; Pint, C. L. Roll-to-Roll Nanomanufacturing of Hybrid Nanostructures for Energy Storage Device Design. *ACS Appl. Mater. Interfaces* **2015**, *7*, 14201−14210.

(11) Choi, H.; Choi, J. S.; Kim, J.-S.; Choe, J.-H.; Chung, K. H.; Shin, J.-W.; Kim, J. T.; Youn, D.-H.; Kim, K.-C.; Lee, J.-I.; Choi, S.-Y.; Kim, P.; Choi, C.-G.; Yu, Y.-J. Flexible Electronics: Flexible and Transparent Gas Molecule Sensor Integrated with Sensing and Heating Graphene Layers. *Small* **2014**, *10*, 3812−3812.

DOI: 10.1021/acsami.5b08171
ACS Appl. Mater. Interfaces 2015, 7, 27215−27222

(12) Kim, S. M.; Song, E. B.; Lee, S.; Zhu, J.; Seo, D. H.; Mecklenburg, M.; Seo, S.; Wang, K. L. Transparent and Flexible Graphene Charge-Trap Memory. *ACS Nano* **2012**, *6*, 7879−7884.
(13) Yang, Y.; Jeong, S.; Hu, L.; Wu, H.; Lee, S. W.; Cui, Y. Transparent Lithium-Ion Batteries. *Proc. Natl. Acad. Sci. U. S. A.* **2011**, *108*, 13013−13018.
(14) Byoung-Joon, A.; Ji-Youp, K.; Sung-Lim, K. Roll-to-Roll Microimprinting Process for Indium Tin Oxide Layer Patterning. *Jpn. J. Appl. Phys.* **2013**, *52*, 05DB09.
(15) Shin, Y.-H.; Kim, H.-K. Effects of Ar Ion Beam Treatment on Properties of Roll-to-Roll Sputtered Sn-Doped In_2O_3 Films on Colorless Polyimide Substrate. *Thin Solid Films* **2014**, *559*, 27−30.
(16) Choi, T.; Kim, S. J.; Park, S.; Hwang, T. Y.; Jeon, Y.; Hong, B. H. Roll-to-Roll Continuous Patterning and Transfer of Graphene via Dispersive Adhesion. *Nanoscale* **2015**, *7*, 7138−7142.
(17) Wang, X.; Zhi, L.; Müllen, K. Transparent, Conductive Graphene Electrodes for Dye-Sensitized Solar Cells. *Nano Lett.* **2008**, *8*, 323−327.
(18) Vosgueritchian, M.; Lipomi, D. J.; Bao, Z. Highly Conductive and Transparent PEDOT:PSS Films with a Fluorosurfactant for Stretchable and Flexible Transparent Electrodes. *Adv. Funct. Mater.* **2012**, *22*, 421−428.
(19) Sam, F. L. M.; Mills, C. A.; Rozanski, L. J.; Silva, S. R. P. Thin Film Hexagonal Gold Grids as Transparent Conducting Electrodes In Organic Light Emitting Diodes. *Laser Photon. Rev.* **2014**, *8*, 172−179.
(20) Wu, Z.; Chen, Z.; Du, X.; Logan, J. M.; Sippel, J.; Nikolou, M.; Kamaras, K.; Reynolds, J. R.; Tanner, D. B.; Hebard, A. F.; Rinzler, A. G. Transparent, Conductive Carbon Nanotube Films. *Science* **2004**, *305*, 1273−1276.
(21) Kim, J.-Y.; Jeon, J.-H.; Kwon, M.-K. Indium Tin Oxide-Free Transparent Conductive Electrode for GaN-Based Ultraviolet Light-Emitting Diodes. *ACS Appl. Mater. Interfaces* **2015**, *7* (15), 7945−7950.
(22) Zhang, D.; Wang, R.; Wen, M.; Weng, D.; Cui, X.; Sun, J.; Li, H.; Lu, Y. Synthesis of Ultralong Copper Nanowires for High-Performance Transparent Electrodes. *J. Am. Chem. Soc.* **2012**, *134*, 14283−14286.
(23) Ahn, Y.; Jeong, Y.; Lee, D.; Lee, Y. Copper Nanowire-Graphene Core-Shell Nanostructure for Highly Stable Transparent Conducting Electrodes. *ACS Nano* **2015**, *9*, 3125−3133.
(24) Deng, B.; Hsu, P.-C.; Chen, G.; Chandrashekar, B. N.; Liao, L.; Ayitimuda, Z.; Wu, J.; Guo, Y.; Lin, L.; Zhou, Y.; Aisijiang, M.; Xie, Q.; Cui, Y.; Liu, Z.; Peng, H. Roll-to-Roll Encapsulation of Metal Nanowires between Graphene and Plastic Substrate for High-Performance Flexible Transparent Electrodes. *Nano Lett.* **2015**, *15*, 4206−4213.
(25) Kim, S.; Kim, S. Y.; Chung, M. H.; Kim, J.; Kim, J. H. A One-Step Roll-to-Roll Process of Stable AgNw/PEDOT:PSS Solution Using Imidazole as a Mild Base for Highly Conductive and Transparent Films: Optimizations And Mechanisms. *J. Mater. Chem. C* **2015**, *3*, 5859−5868.
(26) Lee, M.-S.; Lee, K.; Kim, S.-Y.; Lee, H.; Park, J.; Choi, K.-H.; Kim, H.-K.; Kim, D.-G.; Lee, D.-Y.; Nam, S.; Park, J.-U. High-Performance, Transparent, and Stretchable Electrodes Using Graphene-Metal Nanowire Hybrid Structures. *Nano Lett.* **2013**, *13*, 2814−2821.
(27) Tokuno, T.; Nogi, M.; Jiu, J.; Sugahara, T.; Suganuma, K. Transparent Electrodes Fabricated via the Self-assembly of Silver Nanowires Using a Bubble Template. *Langmuir* **2012**, *28*, 9298−9302.
(28) Wu, H.; Kong, D.; Ruan, Z.; Hsu, P.-C.; Wang, S.; Yu, Z.; Carney, T. J.; Hu, L.; Fan, S.; Cui, Y. A Transparent Electrode Based on a Metal Nanotrough Network. *Nat. Nanotechnol.* **2013**, *8*, 421−425.
(29) Gupta, R.; Rao, K. D. M.; Kulkarni, G. U. Transparent and Flexible Capacitor Fabricated Using a Metal Wire Network as a Transparent Conducting Electrode. *RSC Adv.* **2014**, *4*, 31108−31112.
(30) Gupta, R.; Rao, K. D. M.; Srivastava, K.; Kumar, A.; Kiruthika, S.; Kulkarni, G. U. Spray Coating of Crack Templates for the Fabrication of Transparent Conductors and Heaters on Flat and Curved Surfaces. *ACS Appl. Mater. Interfaces* **2014**, *6*, 13688−13696.
(31) Han, B.; Pei, K.; Huang, Y.; Zhang, X.; Rong, Q.; Lin, Q.; Guo, Y.; Sun, T.; Guo, C.; Carnahan, D.; Giersig, M.; Wang, Y.; Gao, J.; Ren, Z.; Kempa, K. Uniform Self-Forming Metallic Network as a High-Performance Transparent Conductive Electrode. *Adv. Mater.* **2014**, *26*, 873−877.
(32) Kiruthika, S.; Gupta, R.; Kulkarni, G. U. Large Area Defrosting Windows Based on Electrothermal Heating of Highly Conducting and Transmitting Ag Wire Mesh. *RSC Adv.* **2014**, *4*, 49745−49751.
(33) Kiruthika, S.; Gupta, R.; Rao, K. D. M.; Chakraborty, S.; Padmavathy, N.; Kulkarni, G. U. Large Area Solution Processed Transparent Conducting Electrode Based on Highly Interconnected Cu Wire Network. *J. Mater. Chem. C* **2014**, *2*, 2089−2094.
(34) Kiruthika, S.; Rao, K. D. M.; Ankush, K.; Ritu, G.; Kulkarni, G. U. Metal Wire Network Based Transparent Conducting Electrodes Fabricated Using Interconnected Crackled Layer as Template. *Mater. Res. Express* **2014**, *1*, 026301.
(35) Rao, K. D. M.; Gupta, R.; Kulkarni, G. U. Fabrication of Large Area, High-Performance, Transparent Conducting Electrodes Using a Spontaneously Formed Crackle Network as Template. *Adv. Mater. Interfaces* **2014**, *1*, 1400090 DOI: 10.1002/admi.201400090.
(36) Rao, K. D. M.; Kulkarni, G. U. A Highly Crystalline Single Au Wire Network as a High Temperature Transparent Heater. *Nanoscale* **2014**, *6*, 5645−5651.
(37) Gupta, R.; Hösel, M.; Jensen, J.; Krebs, F. C.; Kulkarni, G. U. Digital Grayscale Printing for Patterned Transparent Conducting Ag Electrodes and Their Applications In Flexible Electronics. *J. Mater. Chem. C* **2014**, *2*, 2112−2117.
(38) Mayousse, C.; Celle, C.; Fraczkiewicz, A.; Simonato, J.-P. Stability of Silver Nanowire Based Electrodes Under Environmental and Electrical Stresses. *Nanoscale* **2015**, *7*, 2107−2115.
(39) Rathmell, A. R.; Nguyen, M.; Chi, M.; Wiley, B. J. Synthesis of Oxidation-Resistant Cupronickel Nanowires for Transparent Conducting Nanowire Networks. *Nano Lett.* **2012**, *12*, 3193−3199.
(40) Elechiguerra, J. L.; Larios-Lopez, L.; Liu, C.; Garcia-Gutierrez, D.; Camacho-Bragado, A.; Yacaman, M. J. Corrosion at the Nanoscale: The Case of Silver Nanowires and Nanoparticles. *Chem. Mater.* **2005**, *17*, 6042−6052.
(41) Rycenga, M.; Cobley, C. M.; Zeng, J.; Li, W.; Moran, C. H.; Zhang, Q.; Qin, D.; Xia, Y. Controlling the Synthesis and Assembly of Silver Nanostructures for Plasmonic Applications. *Chem. Rev.* **2011**, *111*, 3669−3712.
(42) Ahn, Y.; Jeong, Y.; Lee, Y. Improved Thermal Oxidation Stability of Solution-Processable Silver Nanowire Transparent Electrode by Reduced Graphene Oxide. *ACS Appl. Mater. Interfaces* **2012**, *4*, 6410−6414.
(43) Moon, I. K.; Kim, J. I.; Lee, H.; Hur, K.; Kim, W. C.; Lee, H. 2D Graphene Oxide Nanosheets as an Adhesive Over-Coating Layer for Flexible Transparent Conductive Electrodes. *Sci. Rep.* **2013**, *3*, 21235−21244.
(44) Kholmanov, I. N.; Domingues, S. H.; Chou, H.; Wang, X.; Tan, C.; Kim, J.-Y.; Li, H.; Piner, R.; Zarbin, A. J. G.; Ruoff, R. S. Reduced Graphene Oxide/Copper Nanowire Hybrid Films as High-Performance Transparent Electrodes. *ACS Nano* **2013**, *7*, 1811−1816.
(45) Lee, D.; Lee, H.; Ahn, Y.; Jeong, Y.; Lee, D.-Y.; Lee, Y. Highly Stable and Flexible Silver Nanowire-Graphene Hybrid Transparent Conducting Electrodes for Emerging Optoelectronic Devices. *Nanoscale* **2013**, *5*, 7750−7755.
(46) Chen, J.; Wiley, B.; McLellan, J.; Xiong, Y.; Li, Z.-Y.; Xia, Y. Optical Properties of Pd-Ag and Pt-Ag Nanoboxes Synthesized via Galvanic Replacement Reactions. *Nano Lett.* **2005**, *5*, 2058−2062.
(47) Zhou, L.; Liu, Z.; Zhang, H.; Cheng, S.; Fan, L.-J.; Ma, W. Site-Specific Growth of AgPd Nanodendrites on Highly Purified Au Bipyramids with Remarkable Catalytic Performance. *Nanoscale* **2014**, *6*, 12971−12980.
(48) Hu, L.; Kim, H. S.; Lee, J.-Y.; Peumans, P.; Cui, Y. Scalable Coating and Properties of Transparent, Flexible, Silver Nanowire Electrodes. *ACS Nano* **2010**, *4*, 2955−2963.
(49) Liu, L.; Yu, Y.; Yan, C.; Li, K.; Zheng, Z. Wearable Energy-Dense and Power-Dense Supercapacitor Yarns Enabled by Scalable

Graphene-Metallic Textile Composite Electrodes. *Nat. Commun.* **2015**, *6*, 7260.
(50) Liu, X.; Chang, H.; Li, Y.; Huck, W. T. S.; Zheng, Z. Polyelectrolyte-Bridged Metal/Cotton Hierarchical Structures for Highly Durable Conductive Yarns. *ACS Appl. Mater. Interfaces* **2010**, *2*, 529−535.
(51) Yu, Y.; Yan, C.; Zheng, Z. Polymer-Assisted Metal Deposition (PAMD): A Full-Solution Strategy for Flexible, Stretchable, Compressible, and Wearable Metal Conductors. *Adv. Mater.* **2014**, *26*, 5508−5516.
(52) Yu, Y.; Zeng, J.; Chen, C.; Xie, Z.; Guo, R.; Liu, Z.; Zhou, X.; Yang, Y.; Zheng, Z. Three-Dimensional Compressible and Stretchable Conductive Composites. *Adv. Mater.* **2014**, *26*, 810−815.
(53) Yu, Y.; Zhang, Y.; Li, K.; Yan, C.; Zheng, Z. Bio-Inspired Chemical Fabrication of Stretchable Transparent Electrodes. *Small* **2015**, *11*, 3444−3449.

DOI: 10.1021/acsami.5b08171
ACS Appl. Mater. Interfaces 2015, 7, 27215−27222